Astron. Astrophys. 339, 187–193 (1998)

ASTRONOMY AND ASTROPHYSICS

Galactic dust polarized emission at high latitudes and CMB polarization

S. Prunet[1], **S.K. Sethi**[2], **F.R. Bouchet**[2], **and M.-A. Miville-Deschênes**[1]

[1] Institut d'Astrophysique Spatiale, Université Paris-Sud, F-91405 Orsay, France
[2] Institut d'Astrophysique de Paris, 98 bis boulevard Arago, F-75014 Paris, France

Received 15 January 1998 / Accepted 31 July 1998

Abstract. With recent instrumental advances, it might become possible to measure the polarization of the Cosmic Microwave Background (CMB), e.g. by future space missions like MAP and Planck Surveyor. In this paper, we estimate the dust polarized emission in our galaxy which is the major foreground to cope with for measuring the CMB polarization in the Wien part of CMB spectrum. We model the dust polarized emission in the galaxy using the three-dimensional HI maps of the Leiden/Dwingeloo survey at high galactic latitudes. We use the fact that the dust emission, for a wide range of wavelengths, has a tight correlation with the HI emission maps of this survey (Boulanger et al. 1996). Assuming the dust grains to be oblate with axis ratio $\simeq 2/3$, which recent studies support, we determine the intrinsic dust polarized emissivity. The distribution of magnetic field with respect to the dust grain distribution is quite uncertain, we thus consider three extreme cases: (1) The magnetic field is aligned with the major axis of the dust structure, (2) the magnetic field has a random direction in the plane perpendicular to the direction of major axis of the dust structure, and (3) the magnetic field is unidirectional throughout. We further assume, as recent observations and theoretical analyses support, that the dust grains align with the magnetic field independently of its strength. The polarization reduction factor from misalignment of the direction of polarization from the plane of the sky and the differential polarization along a line of sight is calculated using these maps, to construct two-dimensional maps of dust polarized emission. We calculate the angular power spectrum of dust polarized emission from these maps and cast it in variables which allow a direct comparison with the polarized component of the CMB. Our results, at frequencies $\simeq 100\,\mathrm{GHz}$, suggest that: (a) This foreground contamination is smaller than the scalar-induced polarization of the CMB at $\ell \gtrsim 200$ while the tensor-induced polarization of CMB, which is an order of magnitude smaller than the scalar-induced polarization, lies below the foreground contamination level for $\ell \gtrsim 200$, (b) the temperature-polarization cross correlation for dust emission is more than an order of magnitude below the CMB signal for $\ell \geq 200$.

Key words: cosmic microwave background – polarization – ISM: clouds – magnetic fields

1. Introduction

The COBE-DMR discovery of CMB anisotropies at angular scales $\gtrsim 7^\circ$ signaled a watershed era in modern cosmology (Smoot et al. 1992, Bennett et al. 1996). Ever since then, the detection of CMB anisotropies has been reported by several other experiments at smaller angular scales (for details, see Bond 1996). Various theoretical studies have shown that a number of cosmological parameters (e.g. Ω_B, h, etc.) can be determined (within the context of a given model) with unprecedented accuracy if the angular power spectrum of CMB is known from a few arc minutes to a few degrees (Jungman et al. 1996). This will become possible with the future satellite missions like MAP and Planck Surveyor. These future missions will also open the possibility of measuring the polarization of CMB and determining its angular power spectrum. Though the fact that the CMB could be polarized was realized long back (Rees 1968), there exist only upper limits on the polarized component of the CMB from observations (Wollack et al. 1993, Partridge et al. 1988, Lubin et al. 1983). It has been shown that the discovery of CMB polarization, along with its angular pattern on the sky, could help determine the surface of last scattering with high precision. It will also complement the information from temperature anisotropies to better determine cosmological parameters by breaking the degeneracy between the temperature quadrupole C_2 and optical depth to the last scattering surface τ (Zaldarriaga et al. 1997).

A major stumbling block in accurately determining the CMB angular pattern, even with low pixel noise and all sky coverage, is the contamination of CMB signal by galactic and extragalactic foregrounds. The extragalactic foregrounds contaminate only the small angular scales which correspond to the size of the extragalactic object or the typical clustering scales of these objects; extragalactic sources can dominate the foreground at a few arc minute scales (e.g. Toffolatti et al. 1998, Bouchet et al. 1995, Tegmark & Efstathiou 1996). The galactic foregrounds, on the other hand, are present at all angular scales. This entails a detailed study of all the galactic sources—dust,

Send offprint requests to: S. Prunet

synchrotron, and free-free emission— of foreground contamination of CMB measurements. It has been shown that for the measurement of CMB temperature anisotropies, experiments operating at multiple frequencies will be successful in separating and subtracting the foreground contamination from the primary CMB signal (for details see Bouchet et al. 1995, Tegmark & Efstathiou 1996, Bouchet & Gispert in prep.). The CMB polarization signal is 10 to 100 times weaker than the temperature anisotropies (Bond & Efstathiou 1984, Zaldarriaga *et al.* 1997). It is not a priori clear whether the polarized component of foregrounds can be subtracted as easily to determine the CMB polarization as is the case for temperature anisotropy. In this paper, we estimate the foreground contamination due to a polarized component of dust emission in the galaxy—which is likely to be the dominant foreground in polarized channels of the high-frequency instrument (HFI) of Planck Surveyor— and its spatial distribution, to address this question.

Like the scalar-induced temperature anisotropies, the scalar-induced anisotropies in the CMB polarization also peak at angular scales $\simeq 1^\circ$ ($\ell \simeq 200$) (Bond & Efstathiou 1984), therefore it is of primary importance to know the foreground contamination at such angular scales. Given the level of CMB polarization, we also need to consider 'clean' parts of the sky at high galactic latitudes where the contamination is minimum. Unfortunately, no data, with sufficient sky coverage at high galactic latitudes, exists for the polarized component of dust emission (for a recent review on far-infrared polarimetry, see Hildebrand 1996). However, we believe that it is possible to construct the polarized component of the dust emission because of the following reasons:

1. All-sky maps of the unpolarized dust emission exist which cover most of the wavelength range from the near-infrared to millimeter wavelengths (Neugebauer et al. 1984, Reach et al. 1995, Hauser et al. 1997) . This in itself is not enough to speculate on the polarization because the polarization depends on various integrated effects along any line of sight while the measured temperature maps give information only of the projected component.
2. The Leiden/Dwingeloo Survey measured the HI emission in the galaxy with 400 velocity templates, and with a large sky coverage, along any line of sight which accurately scanned the differential rotation of the galaxy, thereby providing valuable information on the three-dimensional distribution of HI in the galaxy (Hartmann & Burton 1995). It has been shown that the dust emission at high galactic latitudes correlates extremely well with the HI distribution in our galaxy for a wide wavelength range (Boulanger et al. 1996) and for column densities $N_{\rm HI} \leq 5 \times 10^{20}$.

This information allows us, along with theoretical models of the dust polarized emission in the galaxy, to construct three-dimensional maps of dust emission which can be used to study the spatial distribution of dust polarized emission. In the next section we describe the method of generating polarized dust emission maps in more detail. In Sect. 3 we calculate the power spectra of the dust polarization maps and compare the level of dust polarized contamination with theoretical predictions of CMB polarization. In Sect. 4, we summarize our findings.

2. Method

The Leiden/Dwingeloo survey covers the entire sky north of $\delta \geq -30^\circ$ with a grid spacing of $\simeq 0.5^\circ$ in both longitude and latitude. Therefore it can be used to study features of the foreground emission for angular scales $\simeq 1^\circ$ which is of special interest to CMB studies. In addition it spans the velocity range from $-450\,\mathrm{kms}^{-1}$ to $450\,\mathrm{kms}^{-1}$ with a spectral resolution of $1.03\,\mathrm{kms}^{-1}$ (Hartmann & Burton 1995). As our aim is to use the velocity information to infer distances to structures, we avoid using maps between longitude -10° and 10° because in this case one is looking too close to the galactic centre and the radial velocities from galactic rotation are nearly zero. For similar reasons, regions with longitudes $\simeq 180^\circ$ are also to be avoided. Also the correspondence between velocity and distance to a structure inverts as one passes from the inner galaxy to the outer galaxy, i.e., though a greater velocity corresponds to a greater distance in the inner galaxy, the opposite is true for the outer galaxy. We therefore avoid line of sights close to longitudes $\simeq 90^\circ$ and $\simeq 270^\circ$. It should also be pointed out that the velocity-distance relation is not single valued for lines of sights in the inner galaxy; a given velocity receives contribution from two points at different scale heights. We assume that all the contribution at a given velocity comes from the point at the smaller scale height. It is justified, especially at high galactic latitudes, because the probability of finding a structure at large scale height is exponentially smaller. We use fifteen 15°x15° maps from latitudes between 30° and 75° for our study.

It should be pointed out here that the turbulent velocity of the interstellar medium prevents us from accurately inferring the Galactic HI 3-dimensional structure from the velocity maps at high latitudes. But as we are interested in understanding the *statistical properties* of the dust polarization from these maps, the results should be weakly affected by this assumption. In any case, our uncertainty about the (unknown) turbulence velocity of the HI gas remains smaller than our absence of knowledge concerning the magnetic field distribution (see below).

From the HI maps of Leiden/Dwingloo survey one can construct a model of the three-dimensional dust distribution using the relation between the optical depth for dust emission τ at $\lambda = 250\,\mu\mathrm{m}$ and the HI column density $N_{\rm HI}$ (Boulanger et al. 1996):

$$\frac{\tau}{N_{\rm HI}} = 10^{-25}\,\mathrm{cm}^2 \qquad (1)$$

Boulanger et al. (1996) also showed that the galactic dust emission spectrum can be well fitted with a Planck spectrum with temperature $= 17.5\,\mathrm{K}$ with emissivity proportional to ν^2. We use this spectral dependence of dust emission throughout this paper. The $N_{\rm HI}$–τ correlation remains good for $N_{HI} \leq 5 \times 10^{20}\,\mathrm{cm}^{-2}$ which is typical for high galactic latitudes.

As our aim is to construct two-dimensional maps of the polarized component of dust emission from these three-

dimensional maps of unpolarized emission, we need the following information: (a) the intrinsic dust polarized emissivity, which depends on the type and shape of the grain, (b) the strength and direction of magnetic field in the diffuse cloud, and (c) the polarization reduction factor.

Intrinsic polarized emissivity. The galactic distribution of dust grains can be well understood by the silicate/graphite model, with the volume fraction of graphites between 0.25 and 0.5 of the silicates in the total grain volume (Lee & Draine 1985). Assuming spheroidal grains, Hildebrand & Dragovan (1995) showed that the grains are oblate with the ratio of axis $\simeq 2/3$. Assuming no reduction of polarization, the intrinsic polarized emissivity is $\simeq 30\%$ in this case (Hildebrand & Dragovan 1995). It is also independent of wavelength for $\lambda \gg a$, a being the size of the dust grains. This condition is easily met for the entire wavelength range we consider (for details see e.g. Hildebrand 1988).

Magnetic field. The dust grains align themselves with the magnetic field. To estimate the reduction of polarization from smearing along any line–of–sight, one needs to know the direction and strength of the magnetic field at varying points along the line–of–sight. There is great uncertainty in the direction of the magnetic field relative to dust distribution as the observational evidence show contradictory indications (Myers & Goodman 1991, Goodman et al. 1990). For the purposes of this paper we assume three cases:

(1) The magnetic field is aligned with the major axis of the structure. This case is relevant for dust filaments aligned with the field.
(2) The magnetic field lies in the plane perpendicular to the major axis of the structure, with its direction random in that plane (valid e.g. for helicoidal field around filaments)
(3) The magnetic field has the same direction throughout the three-dimensional map.

Case (2) and (3) correspond to the two extremes of magnetic field distribution. In case (2), the direction of the magnetic field varies from pixel to pixel while it remain the same throughout the map in case (3). Also we assume, as recent observations and theoretical estimates show, that the dust grains are aligned with the magnetic field independent of the strength of the magnetic field (Jones et al. 1992, Sorrell 1995).

Polarization reduction factor. The reduction of intrinsic polarized emissivity due to projection on the sky can be written as (Lee & Draine 1985):

$$\Phi = RF\cos^2\gamma, \tag{2}$$

where R is the Rayleigh reduction factor which gives the reduction of polarization due to the inclination of grain axes about the direction of the magnetic field. As discussed above, we assume perfect alignment of the dust grains with the magnetic field and therefore take $R = 1$ throughout. The $\cos^2\gamma$ factor accounts for the projection of the direction of polarization on the plane of the sky. Using the three-dimensional maps, we calculate this factor by first estimating, for every pixel, the direction of the structure by finding the direction of minimum gradient in the nearest 27 pixels in the four nearest velocity templates, which are taken as slices in 3-dimensional space. After finding the direction of dust structure with respect to the plane of the velocity template, the direction of magnetic field can be fixed for Case (1) and (2) of the magnetic field distribution. The $\cos^2\gamma$ term (γ being the angle between the direction of magnetic field and the plane of the velocity template) can then be easily computed; and by multiplying by this factor, the projected distribution of polarized emission is evaluated for every velocity template. This procedure is used to construct the projected distribution of the Stokes parameters for the first two cases of the magnetic field distribution. For the third case (the magnetic field having the same direction everywhere), we assume, for simplicity, $\cos^2\gamma = 0.5$. F term (Eq. (2)) is the reduction of polarization from summing the contribution of different directions of polarization along any line of sight (Burn 1966). This factor is estimated directly by vectorially adding the contribution from every velocity template along a line of sight. We neglect the effect of differential polarization across the beam in our analysis. Also neglected is the differential Faraday rotation (Burn 1966). Though the differential Faraday rotation can be an important effect on depolarization for the study of radio synchrotron emission ($\nu \lesssim 1\,\mathrm{GHz}$) in the galaxy (Spoelstra 1984), it is completely negligible for the dust polarized emission at much smaller millimeter wavelengths ($\nu \gtrsim 100\,\mathrm{GHz}$) because the Faraday optical depth is proportional to λ^2.

3. Results

An example of two-dimensional $15^\circ\mathrm{x}15^\circ$ maps of Stokes parameters $Q(\overrightarrow{x})$ and $U(\overrightarrow{x})$ are show in Fig. 1 and 2 . The values of the Stokes parameters depend on the choice of the reference frame chosen to define them (Lightman & Rybicki 1979), though the net polarization $P = \sqrt{(Q^2 + U^2)}$ is of course independent of the reference frame. In constructing maps of Q and U, we take the frames of the square maps, for every velocity template, to be the coordinate axes.

3.1. Percentage of polarization

An important indicator to verify the correctness of our method is to compare the distribution of the polarization percentage with existing observations (Hildebrand 1996). A histogram of percentage of polarized component (number of pixels per 0.5% bin) is shown in Fig. 3, averaged over all the maps between latitudes 30^0 and 45^0, for all the three cases of magnetic field distribution. For the first two cases of magnetic field distribution, a comparison of the expected distribution of the percentage of polarization with the results given in Hildebrand (1996) suggests a good agreement if $R \simeq 0.7$–0.8. However, it should be pointed out that the observations reported in Hildebrand (1996) pertain to molecular clouds which could be optically thick. Therefore a comparison of our results which are valid for optically thin dust emission with those results can be misleading, and it is possible that the percentage of polarized dust emission is higher at high galactic latitudes. However, if one assumes the magnetic

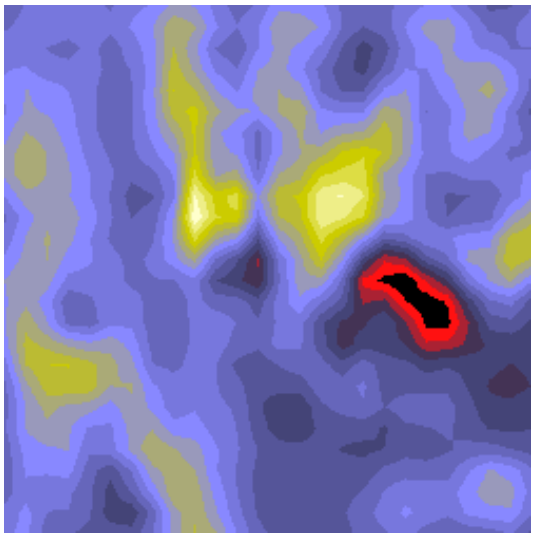

Fig. 1. A 15°x15° map of the Stokes parameter Q, generated using the methods described in Sect. 2.

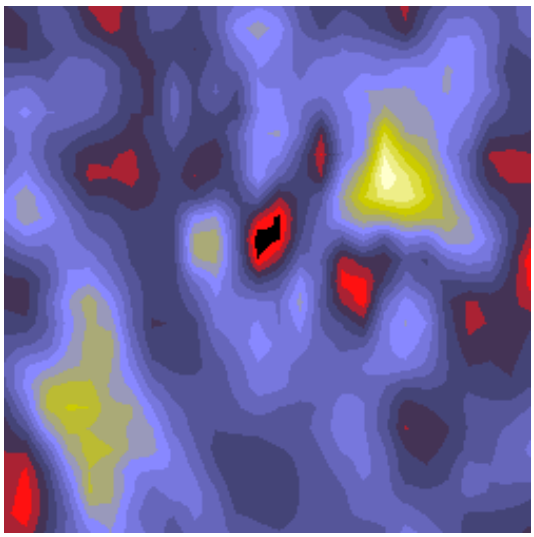

Fig. 2. A 15°x15° map of the Stokes parameter U

field to be constant in direction throughout the map, the resulting distribution of the percentage of polarization is in violent disagreement with observations. We consider this case only as a "toy" model to study the effect of changing the coherence scale of the magnetic field on the spatial distribution of the dust polarized emission.

3.2. Angular distribution of dust polarized emission

The maps of $Q(\overrightarrow{x})$ and $U(\overrightarrow{x})$, constructed using the method described in the previous section, can be directly compared with simulated maps of the CMB. However, the key quantity in studying CMB anisotropies is the angular power spectra of the relevant variables and their cross-correlation. For estimating these quantities, we perform a two dimensional Fourier transform on

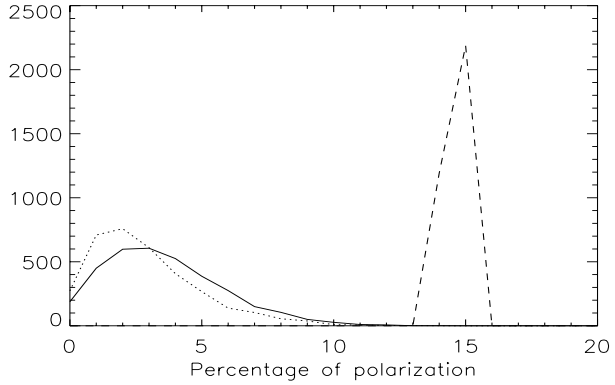

Fig. 3. Distribution of the percentage polarization percentage , averaged over four maps of 15°x15° between latitudes 30° and 45°. The *solid*, *dashed*, and *dotted* lines correspond to Case (1), (2), (3) of the magnetic field distribution (see text), respectively.

the maps and obtain the angular power spectra of the various Stokes parameters defined as:

$$C_T(\ell) = \frac{1}{N}\sum_1^N \left[T(\overrightarrow{l})T^*(\overrightarrow{l})\right] \quad (3)$$

$$C_Q(\ell) = \frac{1}{N}\sum_1^N \left|Q(\overrightarrow{l})Q^*(\overrightarrow{l})\right| \quad (4)$$

$$C_{TQ}(\ell) = \frac{1}{2N}\sum_1^N \left[(Q(\overrightarrow{l})T^*(\overrightarrow{l}) + Q^*(\overrightarrow{l})T(\overrightarrow{l})\right] \quad (5)$$

Here $T(\overrightarrow{l})$ and $Q(\overrightarrow{l})$ are the Fourier transforms of $T(\overrightarrow{x})$ and $Q(\overrightarrow{x})$, respectively; C_U and C_{TU} can likewise be easily defined. N is the number of discrete Fourier modes for each ℓ-bin and $*$ denotes the complex conjugate.

In Figs. 4, 5, and 6 we show the estimated power spectra and cross-correlation between various variables, averaged over all the maps of size 15°x15° between galactic latitudes 30° and 45°. The ℓ dependence of various power spectra does not depend much on the latitude though the normalization decreases by nearly an order from latitudes of 30° to 75°. We recover the $C_T(\ell) \propto \ell^{-3}$ behaviour discussed earlier, among others, by Bouchet et al. (1995), Tegmark & Efstathiou (1996), and Wright (1998). However, the power spectra of Q and U is seen to be much flatter, except in the case of a uni-directional, homogeneous magnetic field. It can be qualitatively understood as follows: the coherence scale of dust structures determines $C_T(\ell)$ while the angular pattern of the polarization variables depends both on the coherent scale of dust structures and the magnetic field; it also depends on the depolarization from smearing along a line of sight. Except in the case of uni-directional, homogeneous magnetic field, the magnetic field has a much smaller coherence scale as compared to the dust structures. An extreme example is the Case (2) of magnetic field distribution in which the magnetic field is almost completely uncorrelated. These effects make the polarization pattern more inhomogeneous, as compared to the unpolarized emission, at small scales, thereby

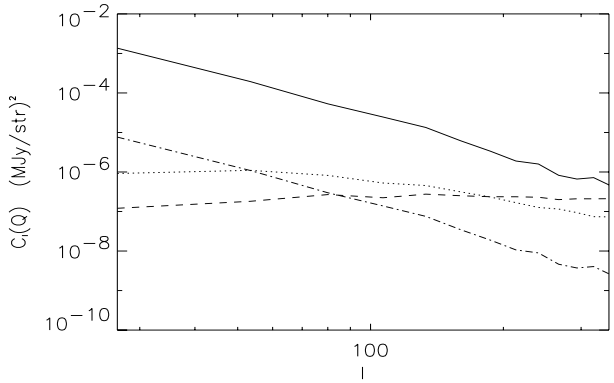

Fig. 4. The power spectra of the Stokes parameter Q are plotted for the three cases of magnetic field distribution at $100\,\mu$m. The *dotted*, *dashed*, and *dot-dashed* lines correspond to Case (1), (2), and (3) of the magnetic field distribution, respectively. The temperature power spectrum (*solid* line) is shown for comparison.

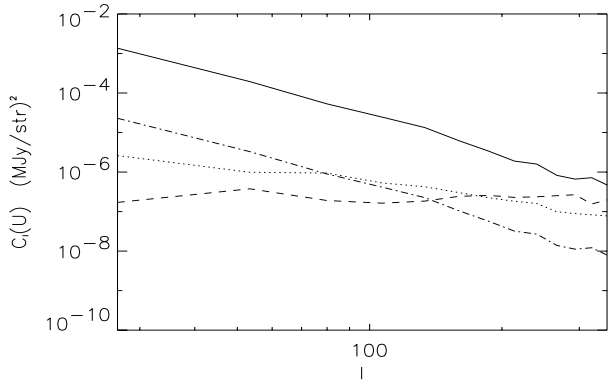

Fig. 5. Same as Fig. 4 for the Stokes parameter U.

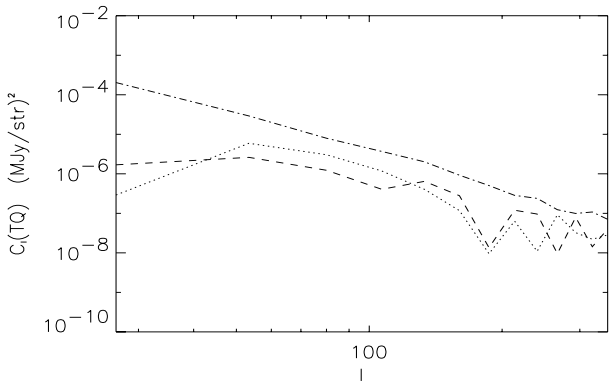

Fig. 6. Same as Fig. 4 for the absolute value of QT cross-correlation power spectrum.

creating more small scale power. This makes the power spectra of Q and U flatter as compared to $C_T(\ell)$.

An interesting interplay between these effects can also be seen in the cross-correlation between Q and T (Fig. 6). In the case of a uni-directional, homogeneous magnetic field, there is a total correlation between T and Q. However, because in this case the cross-correlation power spectrum depends only on the coherence scale of dust structures, it falls as ℓ^{-3}. In the other two cases of magnetic field distribution, the cross-correlation is destroyed by both the depolarization and the small scale magnetic fields; this would explain the lack of large scale power in these cases. However, at $\ell \simeq 100$, the values of cross-correlation power spectra are comparable in all three cases of magnetic field because of the additional small scale power generated in latter two cases. Therefore, our analysis suggests that the $C_{TQ}(\ell)$ should not be very sensitive to the distribution of magnetic field at $\ell \gtrsim 100$, the scales of interest for CMB

3.3. Comparison with CMB power spectra

The dust polarized emission will constitute an important foreground which could severely affect the extraction of CMB signal, especially for CMB experiments operating at frequencies $\gtrsim 100\,\mathrm{GHz}$. The HFI on the future satellite CMB experiment, Planck Surveyor, will attempt to measure the CMB polarization with two channels centered at $143\,\mathrm{GHz}$ and $217\,\mathrm{GHz}$. In addition to these channels, HFI will have a channel at $550\,\mathrm{GHz}$ with polarization capability. In this subsection, we discuss the feasibility of the detection of CMB polarization signal at these frequencies in the presence of galactic foregrounds.

For a comparison with the CMB polarized component, it is convenient to define (Seljak 1997):

$$E(\overrightarrow{l}) = Q(\overrightarrow{l})\cos(2\phi_{\overrightarrow{l}}) + U(\overrightarrow{l})\sin(2\phi_{\overrightarrow{l}}) \quad (6)$$

$$B(\overrightarrow{l}) = -Q(\overrightarrow{l})\sin(2\phi_{\overrightarrow{l}}) + U(\overrightarrow{l})\cos(2\phi_{\overrightarrow{l}}) \quad (7)$$

Here $\phi_{\overrightarrow{l}}$ is solar angle in Fourier space. Seljak (1997) showed that these variable are better for a comparison of foreground polarization with the CMB polarization because B-mode contribution always vanishes for the scalar-induced CMB polarization. Also the cross-correlation of B-mode signal with all the other variables vanishes (for more detail analyses, see Zaldarriaga & Seljak (1996), Kamionkowski et al. 1997). The power spectra and cross-correlations are defined as:

$$C_E(\ell) =$$

$$\frac{1}{N}\sum_1^N \left| Q(\overrightarrow{l})\cos(2\phi_{\overrightarrow{l}}) + U(\overrightarrow{l})\sin(2\phi_{\overrightarrow{l}}) \right|^2 \quad (8)$$

$$C_B(\ell) =$$

$$\frac{1}{N}\sum_1^N \left| -Q(\overrightarrow{l})\sin(2\phi_{\overrightarrow{l}}) + U(\overrightarrow{l})\cos(2\phi_{\overrightarrow{l}}) \right|^2 \quad (9)$$

$$C_{TE}(\ell) =$$

$$\frac{1}{2N}\sum_1^N \Big[\Big(Q(\overrightarrow{l})T^*(\overrightarrow{l}) + Q^*(\overrightarrow{l})T(\overrightarrow{l}) \Big)\cos(2\phi_{\overrightarrow{l}}) +$$

$$\Big(U(\overrightarrow{l})T^*(\overrightarrow{l}) + U^*(\overrightarrow{l})T(\overrightarrow{l}) \Big)\sin(2\phi_{\overrightarrow{l}}) \Big] \quad (10)$$

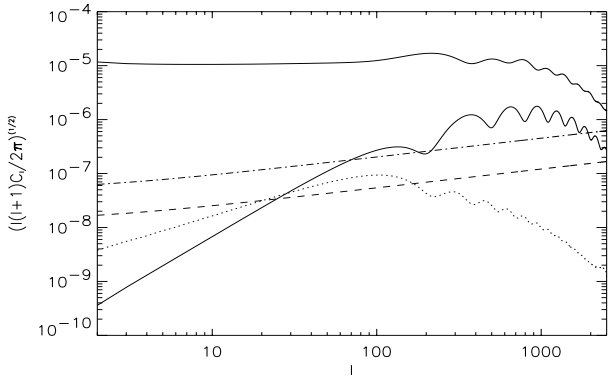

Fig. 7. The power spectra of dust polarized emission is compared with the theoretical predictions for CMB polarization. The scalar and tensor-induced E-mode power spectra (*solid* and *dotted* lines respectively) are plotted against the dust polarized power spectra at $143\,\mathrm{GHz}$ and $217\,\mathrm{GHz}$ (the *dashed* and *dot-dashed* lines, respectively). The CMB temperature power spectrum is shown for comparison (*thick solid* line). The power spectra are plotted in the units of $\Delta T/T$.

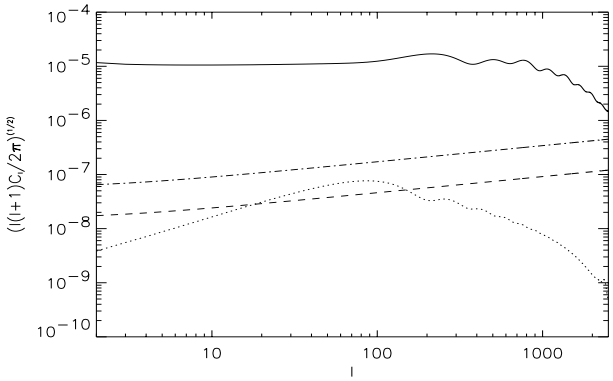

Fig. 8. Same as Fig. 7 for B-mode power spectra. The scalar-induced B-mode power spectrum is identically zero.

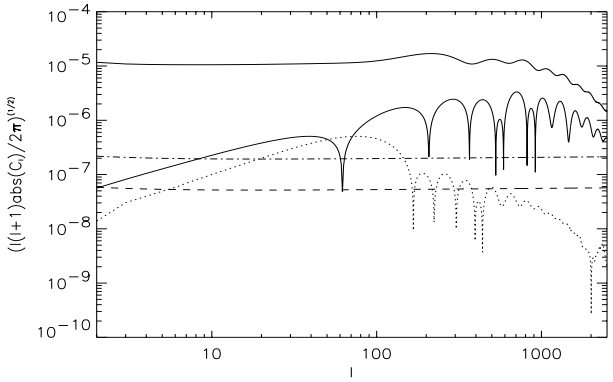

Fig. 9. Same as Fig. 7 for the absolute value of ET cross-correlation.

In terms of these variables, the estimated power spectra and the cross-correlation of dust polarized emission can approximately be fitted by:

$$C_E(\ell) \;=\; 8.9\times10^{-4}\ell^{-1.3}\;(\mu\mathrm{K})^2 \tag{11}$$

$$C_B(\ell) \;=\; 1.0\times10^{-3}\ell^{-1.4}\;(\mu\mathrm{K})^2 \tag{12}$$

$$C_{ET}(\ell) \;=\; 1.7\times10^{-2}\ell^{-1.95}\;(\mu\mathrm{K})^2. \tag{13}$$

The power spectra are normalized at $100\,\mathrm{GHz}$ and are for the maps between galactic latitudes 30° and 45° (where the level of contamination is the highest) for Case (1) of the magnetic field distribution.

We plot these against the scalar- and tensor-induced CMB power spectra for various variables in Fig. 7, 8, and 9. The cosmological model we adopted to compute the CMB spectra is a flat, tilted CDM model, which generates tensor-induced B-mode polarization, with scalar spectral index $n_s = 0.9$. We take the tensor spectral index $n_t = 1-n_s = 0.1$ with scalar to tensor quadrapole ratio of $7(1-n_s)$. The CMB power spectra were computed using the CMB Boltzmann code CMBFAST (Seljak & Zaldarriaga 1996).

In Fig. 7, the scalar-induced E-mode CMB power spectrum is seen to be above the level of dust contamination for $\ell \gtrsim 200$ for the two HFI frequency channels at $143\,\mathrm{GHz}$ and $217\,\mathrm{GHz}$. However the tensor-induced E-mode CMB fluctuations, which in any case constitute a small part of the E-mode signal, are likely to be swamped by the foreground contamination. The detection of B-mode anisotropies is more interesting as it would unambiguously determine the presence of tensor-induced component in CMB fluctuations (see Seljak 1997, Kamionkowski & Kosowsky 1997 and references therein). As seen in Fig. 8 the B-mode power spectrum is at best comparable to the foreground level in a small ℓ-range. Fig 9 shows that the CMB E-T cross-correlation power spectrum from scalar perturbations is more than an order of magnitude above the level of foreground contamination, at least for $\ell \gtrsim 100$ while the tensor-induced E-T cross-correlation remains below the foreground signal.

However, the level of foreground emission shown Fig. 7, 8, and 9 correspond to regions between latitudes 30° and 45°, which is the worst possible case studied here. At higher galactic latitudes (for maps from 60° to 75°), the galactic dust emission is smaller by nearly an order of magnitude. Therefore, it might be possible to detect the tensor-induced CMB polarization signal by deep imaging (to reduce noise) a part of the sky at high galactic latitudes, though such a measurement might be hampered by cosmic variance.

Also, it is important to note that the foregrounds differ from CMB in both ν- and ℓ-dependence. This fact can be used to reduce the level of foreground contamination substantially even in the presence of noise (for details of this multi-frequency Wiener filtering technique for extraction of CMB temperature power spectrum see Bouchet et al. 1995, Tegmark & Efstathiou 1996). The HFI on Planck Surveyor will have a channel at $550\,\mathrm{GHz}$ which will be used to study the spatial distribution of both unpolarized and polarized dust emission in the galaxy, as the dust emission is much larger than the CMB signal at this frequency. Though the instrumental noise in this channel would be higher as compared to the smaller frequency channels of HFI, it might be possible to usefully extrapolate the observations at this channel to lower frequencies, to gauge the level of dust contamination at frequencies where the CMB signal will dominate. To

get quantitative estimates of errors in various power spectra in the presence of foregrounds, we are currently working on the extension of the multi-frequency Wiener filtering technique to include the CMB polarization and cross-correlation.

4. Conclusions and discussion

The detection of CMB polarization is an important goal of future satellite missions. While such a measurement is important in itself, the measurement of CMB polarization will give important clues on the structure of last scattering surface. Furthermore, this measurement helps in a better determination of cosmological parameters by removing the degeneracy between the temperature quadrupole and the optical depth to the last scattering surface.

The major obstacle in measuring CMB polarization is galactic polarized foregrounds. We estimated the dust polarized emission—one of the major foreground—in the galaxy and compared it to the expected CMB polarization signal. This exercise is important for the future CMB experiments like Planck Surveyor's HFI which will try to detect the CMB polarization at frequencies $143\,\mathrm{GHz}$ and $217\,\mathrm{GHz}$. Our results suggest that the expected scalar-induced E-mode signal and the E-T cross-correlation power spectrum are likely to be well above the dust contamination level for $\ell \geq 100$ at the frequencies relevant for the Planck Surveyor. This is particularly true of the CMB E-T cross correlation signal, which should be more than an order of magnitude above the dust polarized emission. The tensor-induced polarization signal, however, is less likely to be disentangled from the foregrounds.

Our analysis showed that the power spectrum of dust polarized emission at large scales (small ℓ) is sensitive to the large scale distribution of magnetic field in the galaxy. The $550\,\mathrm{GHz}$ channel of HFI may succeed in either detecting this signal or in putting useful upper bounds. This could help unravel the magnetic field structure of our galaxy. Such a study might also become possible with the launch of proposed satellite missions like the Polarimeter Infrared Explorer (for details, see Clemens 1996).

Though the dust polarized emission will be the main foreground for high frequency Planck channels, the foregrounds for small frequency experiments like the ground-based POLAR (Keating et al. 1997), satellite experiment MAP, and the low-frequency instrument on Planck Surveyor will be dominated by galactic synchrotron emission. Can we anticipate something about that foreground from the exercise in this paper? Unlike estimating the dust polarized emission, which is greatly facilitated by the dust-HI correlation and the existing three-dimensional HI map, we do not have much information about the three-dimensional structure of the synchrotron emission. This synchrotron emission is sensitive to both the spatial distribution of magnetic field (both strength and direction) and the cosmic ray particles which have to be simulated based on scanty information available about them. An alternative approach would be to work directly with the Leiden polarized maps of the Stokes parameter Q and U analysed by Spoelstra (1984). Work is in progress in this direction.

Acknowledgements. One of us (SP) would like to thank Jean-Loup Puget for several useful suggestions and encouragement. We are thankful to Nabila Aghanim for suggestions on the manuscript.

References

Bennett C.L., Banday A.J., Gorski K.M., et al., 1996, ApJ 464, L1
Bond J.R. 1996, Observations of Large-Scale Structure in the universe, Ed. Schaeffer, R., Les Houches, Elsevier Science Publishers
Bond J.R., Efstathiou G. 1984, ApJ 285, L45
Burn B.J. 1966, MNRAS 133, 67
Bouchet F.R., Gispert R., Aghanim N., et al., 1995, Space Science Rev. 74, 37
Boulanger F., Abergel A., Bernard J.-P., et al., 1996, A & A 312, 256
Clemens D., 1996, ASPC series vol. 97, ed. W. G. Roberge and D. C. B. Whittet
Goodman A.A., Bastien P., Menard F., Myers P.C. 1990, ApJ 359, 363
Hartmann D., Burton W.B., 1995, Atlas of Galactic HI emission, Cambridge University Press
Hauser M.G., Kersall T., Arendt R.G., et al., 1997, DIRBE Explanatory Supplement, COBE Ref. Pub. No. 97-A (Greenbelt, MD: NASA/GSFC)
Hildebrand R.H., 1996, ASPC series vol. 97, ed. W. G. Roberge and D. C. B. Whittet
Hildebrand R.H., Dragovan M. 1995, ApJ 450, 663
Hildebrand R.H., 1988, QJRAS 29, 277
Jones T.J., Klebe K., Dickey J.M., 1992, ApJ 389, 602
Jungman G., Kamionkowski M., Kosowsky A., Spergel D.N., 1996, Phys. Rev. D 54, 1332
Kamionkowski M., Kosowsky A., 1997, astro-ph/9705219
Kamionkowski M., Kosowsky A., Stebbins A., 1997, Phys. Rev D 55, 7368
Keating B., Timbie P., Polnarev A., Steinberger J., 1997, astro-ph/9710087
Lee H.M., Draine B.T., 1985, ApJ 290, 211
Lubin P.M., Melese P., Smoot G.F., 1983, ApJ 273, L51
Lightman A.P., Rybicki G.B., 1979, *Radiative Processes in Astrophysics* (Wiley-Interscience, New York)
Myers P.C., Goodman A.A., 1991, ApJ 373, 509
Neugebauer G., Habing H.J., Van Duinen R., et al., 1984, ApJ 278, L1
Partridge R.B., Nowakowaki J., Martin H.M., 1988, Nat 331, 146
Reach W.T., Dwek E., Fixsen D.J., et al., 1995, ApJ 451,188
Rees M., 1968, ApJ 153, L1
Seljak U., 1997, ApJ 482, 6
Seljak U., Zaldarriaga M., 1996, ApJ 469, 437
Smoot G., Bennett C.L., Kogut A., et al., 1992, ApJ 396, L1
Sorrell W.H., 1995, MNRAS 272, 127
Spoelstra T.A.T., 1984, A & A 135, 238
Tegmark M., Efstathiou G., 1996, MNRAS 281, 1297
Toffolatti L., Argueso Goméz F., De Zotti G., et al., 1998 MNRAS, 297, 117
Wollack E.J., Jarosik N.C., Netterfield C.B., Page L.A., Wilkinson D., 1993, ApJ 419, L49
Wright E.L. 1998, ApJ 496, 1
Zaldarriaga M., Spergel D. N., Seljak U., 1997, ApJ 488, 1
Zaldarriaga M., Seljak U., 1996, astro-ph/9609170